RSC Advances

PAPER

View Article Online
View Journal | View Issue

Cite this: *RSC Adv.*, 2024, **14**, 28741

Characterization of dolomite and calcite microcalcifications in human breast tissue†

Sahar Gal,[a] Mariela J. Pavan[b] and Netta Vidavsky *[ab]

Pathological crystallization within soft tissues often yields biominerals with properties differing from those of their geological or synthetic counterparts. Microcalcifications (MCs) are abundant in breast tumors, particularly in non-invasive lesions, such as ductal carcinoma *in situ* (DCIS). Given the challenge of predicting DCIS progression into invasive cancer, it has been suggested that MCs can be leveraged to inform DCIS prognosis. The predominant type of breast MCs are those containing calcium phosphates (CaP), whose crystal properties are commonly held to correlate with malignancy. Less common are non-CaP minerals, which have received less attention, as they are associated mainly with benign lesions. Here, we conducted a retrospective study of tissue samples collected from patients who were originally diagnosed with DCIS and whose current medical status is known. We examined the elemental composition, morphology, and crystal phases of 398 MCs, aiming to investigate potential correlations between MC crystal properties and the progression of DCIS. Our findings revealed primarily non-CaP MCs, an observation that was likely made possible only by the tissue processing methodology employed, which did not involve harsh conditions. We found that non-CaP MCs were abundant in DCIS lesions, that they exhibited diverse morphologies and sizes, and that they were composed of calcite and dolomite. Dolomite formation in cancer has not been reported previously and may be linked to pH fluctuations in the tumor microenvironment. The small size of DCIS lesions often requires pathologists to use the entire sample, thus reducing the number of samples available for further research. Nonetheless, despite our limited sample size, the observed trend indicated an association of dolomite MCs with DCIS lesions that progressed into invasive cancer over time.

Received 5th June 2024
Accepted 3rd September 2024

DOI: 10.1039/d4ra04137b

rsc.li/rsc-advances

1. Introduction

Breast cancer begins primarily in the milk ducts or lactiferous ducts, and in the initial phase of abnormal growth cancerous mammary cells proliferate within these ducts. As long as the cells remain confined within the ducts, they are regarded as being in a non-invasive stage, known as ductal carcinoma *in situ* (DCIS).[1,2] The most common method for detecting DCIS is the identification of calcium deposits, known as microcalcifications (MCs), *via* mammography.

These MCs can be observed not only in DCIS and invasive cases but also in benign conditions like oil cysts and some vascular calcifications. However, specific patterns in their spatial distribution, morphology, and size are linked to a higher likelihood of malignancy.[3] A high prevalence of MCs characterizes breast cancer, with DCIS being the breast cancer subtype most frequently associated with them. In particular, fine pleomorphic MCs, as well as fine linear and fine linear branching MCs, are associated with high-grade DCIS.[4] Despite extensive efforts to improve the prognosis of DCIS based on biomolecular and histoclinical characteristics, it is currently impossible to predict whether DCIS will develop into invasive ductal carcinoma (IDC).[5,6] Therefore, although it is estimated that only up to 53% of DCIS cases will develop into IDC,[6–9] the standard of care is to treat DCIS as if it would develop into IDC, often leading to surgical interventions, with associated side effects and negative long-term health impacts.[10,11] This highlights the need to develop new protocols to de-escalate DCIS overtreatment.

Among the various types of MCs – differing in their chemical composition and crystal phase and morphology[12–15] – found in breast tissue, the most commonly observed MCs are those composed of calcium phosphate (CaP). These MCs consist primarily of carbonated apatite, $(Ca)_{10}(PO_4,CO_3)_6(OH)_2$, and a magnesium-substituted beta-tricalcium phosphate known as whitlockite, $(Ca,Mg)_3(PO_4)_2$.[3,13,14,16–19] Numerous studies have investigated the crystal properties of these CaP MCs and their relationship with malignancy, highlighting associations with crystallinity and/or the presence of carbonate, sodium, zinc, and magnesium;[3,12–15,19–22] for example, the presence of

[a]*Department of Chemical Engineering, Ben-Gurion University of the Negev, Beer-Sheva 8410501, Israel. E-mail: nettav@bgu.ac.il*

[b]*Ilse Katz Institute for Nanoscale Science & Technology, Ben-Gurion University of the Negev, Beer-Sheva 8410501, Israel*

† Electronic supplementary information (ESI) available. See DOI: https://doi.org/10.1039/d4ra04137b

magnesium in apatitic MCs has been associated with more malignant breast tumors,[20,21,23] and there are various reports of associations of whitlockite with breast malignancy, often invasive cancers.[14,15,18,20,24]

A less frequently observed group of breast MCs are those that lack phosphate (designated non-CaP), which are less well studied. Among these, calcium oxalate dihydrate ($CaC_2O_4 \cdot (H_2O)_2$) MCs are the best known and are associated primarily with benign conditions rather than cancerous conditions or DCIS.[17,20,25,26] Additionally, individual very small birefringent calcium carbonate crystals, particularly calcite ($CaCO_3$), have been identified in breast tissue, but currently the existing data is insufficient to explain any association with pathology.[14,24,27]

Despite their high prevalence and diverse properties, breast MCs are currently used only for breast cancer screening, based on their appearance in mammograms, and their crystal properties are not utilized to inform the prognosis of DCIS.[3,10] Nonetheless, the crystal properties of MCs, including morphology, structure, chemical composition, and size, may hold crucial information about DCIS characteristics that could lead to improved disease prognosis and aid in treatment decisions.

While previous studies have focused mainly on CaP MCs, our study investigates the relationship between the properties of non-CaP MCs and the progression of DCIS into IDC. Here, we present a retrospective study of biopsy samples obtained from patients diagnosed with DCIS, each exhibiting different stages of disease progression and clinical outcomes. Fresh, flash-frozen breast tissue samples were collected from these DCIS patients as part of a biopsy procedure, and in our study the subsequent treatment of the tissue samples was as minimal as possible so as to preserve the crystal properties. A relationship was then sought between the characteristics of the non-CaP MCs (crystal phase, chemical composition, size and morphology) and disease outcomes.

2. Materials and methods

2.1 Study design

A retrospective study was conducted on breast tissue samples obtained from the Israeli Biorepository Network for Research (MIDGAM). The samples had been collected between 2014 and 2020 as part of a biopsy procedure from six patients, who had been diagnosed with DCIS between the years 2014 and 2019. This study was conducted in accordance with the Declaration of Helsinki and the Israeli Public Health Regulations (Medical Experiments on Humans, 1980) and was approved by the Israeli Biorepository Network for Research (MIDGAM) institutional review committee (MID-034-202). The patients had provided informed consent, and the study was conducted according to the approved Helsinki study protocol.

The study inclusion criteria were female patients aged ≥18 years who had undergone a biopsy procedure for DCIS. Pregnant women and women with infections were excluded from the study. Following the pathological evaluation, the remaining tissue had been flash-frozen and stored at −80 °C. The diagnosis made by a certified pathologist was provided to us along with the tissue samples. The patients exhibited different degrees of disease progression and different clinical outcomes. Patient information was anonymized, and codes were assigned for analysis.

The six patients received different treatment protocols based on their physicians' assessments of their overall clinical status. Their treatments included either lumpectomy or mastectomy and, in some cases, sentinel lymph node excision. They also underwent one or more of the following: radiation therapy, hormonal therapy, biological therapy, and chemotherapy. Some patients received treatment both before and after tissue collection, while others had treatment only after collection.

The study design was planned to include two types of tissue for each patient—tumorous tissue, taken from the area of the cancerous lesion within the patient's breast, and healthy, non-tumorous tissue obtained from a nearby healthy, non-cancerous region beyond the area of the lesion. These two tissue types were characterized for four out of six patients. Out of these four patients, the DCIS progressed to IDC over time in two, but in the other two, it did not progress. We classify DCIS cases as either "developed" or "undeveloped." "Developed DCIS" refers to cases where medical records from several years after diagnosis indicate the progression to IDC. "Undeveloped DCIS" refers to cases where no invasive cancer was detected in the subsequent years.

For the remaining two patients, the DCIS did not progress over time. For one patient out of these two, only a cancerous tissue sample was available, and for the second patient, both normal and cancerous samples were available, but the normal tissue sample was used for preliminary experiments to support the experimental design and protocol development and optimization. For the second patient, the tissue samples were obtained in 2020 although the diagnosis of DCIS had been made in 2017. Patient characteristics are presented in Table S1.† The data, collected by the patient's attending physician, included: illness diagnosis date, illness stage, tumor grade, pathological and clinical diagnosis, surgery performed on the patient, tumor size, post-operative treatment, BRCA, HER2, PR and ER status, the Ki67 marker, and outcome and follow-ups updated to December 2021. Information on age, height, weight, BMI, ethnicity, birth country, and smoking habits is also included in Table S1.†

2.2 Sample size considerations

Owing to the small size of DCIS tumors, there is often no more material available for analysis after the routine pathological evaluation has been completed, and therefore the number of DCIS patients included in this study was limited by the lack of material. The research design was originally planned for identification of a minimum of 20 MCs within the two tissue types of each patient. Although the final number of MCs analyzed was a substantial total of 398 (see Results), it was not possible to perform meaningful statistical analysis of the results, due to the small number of patients in the study.

2.3 Tissue processing

Upon receipt of the frozen tissues in our laboratory, the material was quickly transferred to a mold (Tissue-Tek biopsy cryomold,

Sakura Finetek, Torrance, CA, USA), immersed in optimal cutting temperature compound (OCT; Scigen Scientific, Gardena, CA, USA), and refrozen at −20 °C either in a freezer or within a Leica CM3050 S cryostat (Wetzlar, Germany) for at least 30 min before sectioning. The tissue samples were then sectioned into thin 16 μm sections with a cryostat operating at −20 °C. If the tissue samples exhibited slight tearing at the selected thickness, they were sectioned in a slightly thicker range of 18–20 μm to preserve the spatial structure. During the cryo-sectioning procedure, each tissue section was mounted on a charged glass slide (Bar-Naor Adhesion microscope slides, BN9308c, Petah Tikva, Israel) or on aluminum foil, according to the type of characterization planned, and air dried. To ensure that the tissue sections were no longer biohazardous, they were fixed in 4% paraformaldehyde (Thermo Scientific Chemicals, Waltham, MA, USA) in phosphate-buffered saline (PBS; 1×, Sigma-Aldrich, St. Louis, MO, USA) for 10 min, followed by two PBS washings for 10 min each. For each sample, three sets of sequential tissue sections were prepared: one on a glass slide and two on aluminum foil. Each set of three sequential tissue sections was subjected to our characterization protocol and analysis, as shown in Fig. 1. In contrast to conventional paraffin embedding and sectioning methods, flash-freezing followed by cryo-sectioning eliminated the need for solvents or heating, reducing the likelihood of displacement or alteration of the crystal structure of mineral particles within the tissue.

2.4 Tissue and MC characterization

2.4.1 Light microscopy. Light microscopy was performed to visualize the tissue structure and confirm the presence of embedded MCs in their original spatial context. Tissue sections mounted on glass slides were observed under a light microscope equipped with cross polarizers (Nikon Eclipse Ci-L Ergo upright microscope, NY, USA) and a color camera (DS-Fi3 digital camera), enabling visualization of the tissue structure and localization of MCs within their original spatial context. Adobe Photoshop (version 24.1) was used for contrast and brightness adjustments. Image processing was performed consistently for all the conditions.

2.4.2 Scanning electron microscopy and energy dispersive X-ray spectroscopy (SEM-EDS). High-resolution field emission SEM (Verios 460L, Thermo Fisher Scientific, Waltham, MA, USA) was used for characterization of the size and morphology of the MCs in each tissue section and for determination of their elemental composition. Tissue sections mounted on aluminum foil were affixed to SEM aluminum stubs using PELCO® Conductive Graphite (Ted Pella, Inc., Redding, CA, USA). Then, the tissue sections were sputter-coated with carbon to a thickness of 10 nm using a Quorum Q150T ES (Quorum Technologies, UK) instrument. Initially, a secondary electron detector with a low accelerating voltage (3–5 kV) was used to locate 'lumps' and abnormal clusters within the tissue, namely, potential MCs embedded in the sample. Additionally, a back-scattered electron detector was used to identify materials containing elements with high atomic numbers, such as minerals, further aiding in the identification of MCs. Putative MCs were imaged to determine their size and morphology, followed by EDS elemental analysis at a higher accelerating voltage (10 kV). The elemental composition analysis excluded aluminum and silicon, as aluminum originated from the substrate, and silicon, most likely, from external impurities. Elemental composition was calculated using AZtec 2.1 software (Oxford Instruments). Adobe Photoshop (version 24.1) was used for contrast and brightness adjustments. Image processing was performed consistently for all conditions.

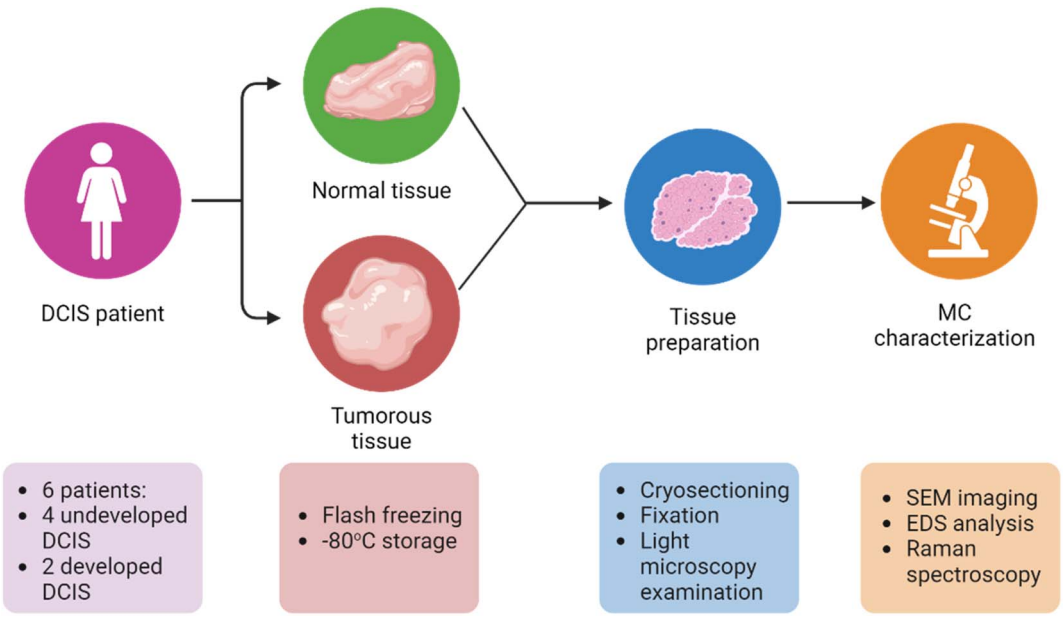

Fig. 1 Overall experimental design. MC characterization included scanning electron microscopy (SEM) imaging, energy dispersive X-ray spectroscopy (EDS) analysis, and Raman spectroscopy.

2.4.3 Raman spectroscopy. Raman spectroscopy was utilized to analyze the composition and crystal phases of the MCs present in tissue sections mounted on the aluminum-covered slides. The samples were first scanned using cross-polarized white light to identify birefringent particles. Micro-Raman measurements were acquired with a confocal Horiba LabRam HR evolution instrument, equipped with a Syncerity CCD detector (deep-cooled to −60 °C, 1024 × 256 pixels). The excitation source was a Nd:YAG 532 nm laser with a power of 3.5 mW. The laser was focused on the MCs with a 50× LWD objective (Olympus LMPlanFL-N, NA = 0.5) or a 100× objective (MPLN100×, NA = 0.9) to a spot size of 1.3 or 0.7 μm, respectively. The measurements were obtained using a 600 g mm^{-1} grating and a confocal hole ranging from 70 to 100 μm. The typical exposure time was 10 s. LabSpec software (version 6.5.2.11) was used to operate the equipment and for data processing (baseline correction). Initial identification was performed using the KnowItAll Raman Spectral Database (KnowItAll Informatic System 2023, John Wiley Sons, Inc.). Plotting and spectral analysis were performed using Origin Pro 2020 software. Peak locations were determined based on second derivative analysis using Origin Pro 2020.

2.5 Calcite and magnesium-calcite standards

Commercial calcite (Merck, Darmstadt, Germany) and lab-synthesized magnesium-calcite were used as standards for the Raman spectroscopy analysis. Magnesium-calcite was synthesized by quickly mixing 200 mL of a 2 M Na_2CO_3 solution (Sigma-Aldrich, St. Louis, MO, USA) with 10 mL of a 0.1 M $MgCl_2$ solution (Sigma-Aldrich) and 5 mL of a 0.1 M $CaCl_2$ solution (Fisher Scientific, Loughborough, UK) at room temperature. The resulting suspension was stirred continuously at 100 rpm for 1 h, after which it was centrifuged. The precipitate was filtered off under vacuum, washed with deionized water (Direct-Q Water Purification System, resistivity of 18 MΩ) and ethanol, and dried at 40 °C in a drying oven. The composition and crystal phase of the product were verified by EDS and Raman spectroscopy.

3. Results

We ensured that every MC originated from the tissue by following specific SEM-EDS and Raman analysis procedures. In SEM-EDS, we consistently observed the surroundings of the MCs, often in the proximity of an organic matrix. However, for some MCs, it was challenging to discern the degree of integration of MCs into the tissue solely through imaging, and, therefore, occasional EDS measurements were conducted on the periphery of the MCs to validate the absence of aluminum (the substrate material) and to ensure an accurate identification of tissue-derived MCs.

In the Raman analysis, we consistently encountered challenges in focusing on the MCs due to their varying orientations and depths within the tissue. This difficulty provided compelling evidence that the MCs were indeed embedded within the tissue matrix, rather than a potential result of surface contamination. To rule out potential false identifications, we acquired spectra from birefringent particles located outside the tissue, including those on the aluminum substrate and suspected OCT residues, all of which were confirmed not to be MCs. In addition, for both Raman and SEM-EDS techniques, analyses were also conducted on OCT sections to ensure the absence of calcium-containing particles that might have been adhered to the tissue sections during sectioning and fixation.

We analyzed a total of 398 individual MCs embedded in either tumorous or normal breast tissue (Table 1). SEM-EDS imaging and analysis were conducted on 201 MCs, comprising 104 MCs from patients with developed DCIS (51.7%) and 97 MCs from those with undeveloped DCIS (48.3%). Additionally, Raman spectroscopy and analysis were carried out on 197 MCs, with 94 MCs from developed DCIS patients (47.7%) and 103 MCs from undeveloped DCIS cases (52.3%).

3.1 MC morphology

To provide a comprehensive description of breast MCs, we used SEM imaging to define several morphology categories, including spongy particles, aggregates (both loose-packed and

Table 1 Quantification and categorization of the MCs analyzed in this study by clinical outcome, tissue type, and characterization method

	SEM imaging + EDS analysis			Raman spectroscopy		
	MCs analyzed in healthy tissue	MCs analyzed in tumorous tissue	Total MCs analyzed	MCs analyzed in healthy tissue	MCs analyzed in tumorous tissue	Total MCs analyzed
Developed DCIS						
Patient 1	44	14	**58**	25	32	**57**
Patient 2	21	25	**46**	20	17	**37**
Undeveloped DCIS						
Patient 3	5	19	**24**	29	22	**51**
Patient 4	—	23	**23**	—	23	**23**
Patient 5	25	4	**29**	4	4	**8**
Patient 6	—	21	**21**	—	21	**21**
Total for all patients			**201**			**197**

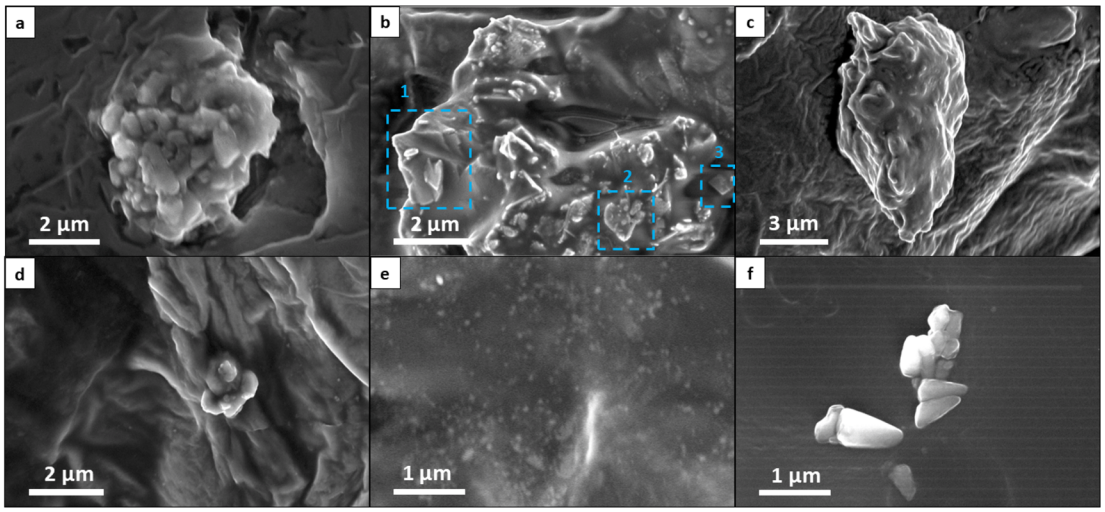

Fig. 2 SEM images of MCs, exhibiting various morphologies and particle sizes, embedded in breast tissue sections. The following morphologies are shown: (a and b) Loose-packed aggregate: (b1) faceted, (b2) spongy, (b3) prism (orthorhombic), (c) dense aggregate, (d) spongy, (e) punctulate, and (f) prism (wedge).

dense), particles with prismatic, faceted or punctulate morphologies, and tiny particles (Fig. 2 and 3a). These categories were inspired by the existing lexicon of terms used for breast MCs in mammography and by advances in the classification of breast MC micromorphology.[28]

In our classification system, aggregates represent the clustering of distinct particles. Typically, aggregates are larger than particles of other morphologies, and they can be further categorized into sub-morphologies discernible through high-voltage secondary electron detection or backscattered electron detection. Loose-packed aggregates (Fig. 2a and b) of various morphologies contain interconnected or closely positioned particles with clearly visible borders. Dense aggregates are typically larger than loose aggregates and have smooth surfaces (Fig. 2c). The sub-particles of these dense aggregates can be observed only through high accelerating voltage imaging. Some aggregates may display multiple sub-morphologies, reflecting diverse domains within different spatial regions of the MCs. Faceted particles are composed of thin layers with smooth surfaces and sharp angular edges (Fig. 2b1). Spongy particles are uniform masses, often with rounded edges, that are characterized by porous structures and irregular lumpy surfaces (Fig. 2b2 and d). These particles are smaller than aggregates and do not exhibit sub-morphologies or sub-particles, even under high accelerating voltage imaging. Punctulate MCs are comprised of many sub-micrometer dots dispersed over a wide area that is at least an order of magnitude larger than that of an individual dot (Fig. 2e). Prismatic particles constitute a highly organized category of particles characterized by distinct morphologies—tetrahedral, orthorhombic, rod-shaped, and wedge-shaped (Fig. 2f). Finally, tiny particles refer to individual MCs whose morphology is not distinctly discernible due to their small size (less than 0.8 µm). These tiny particles were identified as MCs on the basis of their elemental composition, as determined by EDS analysis.

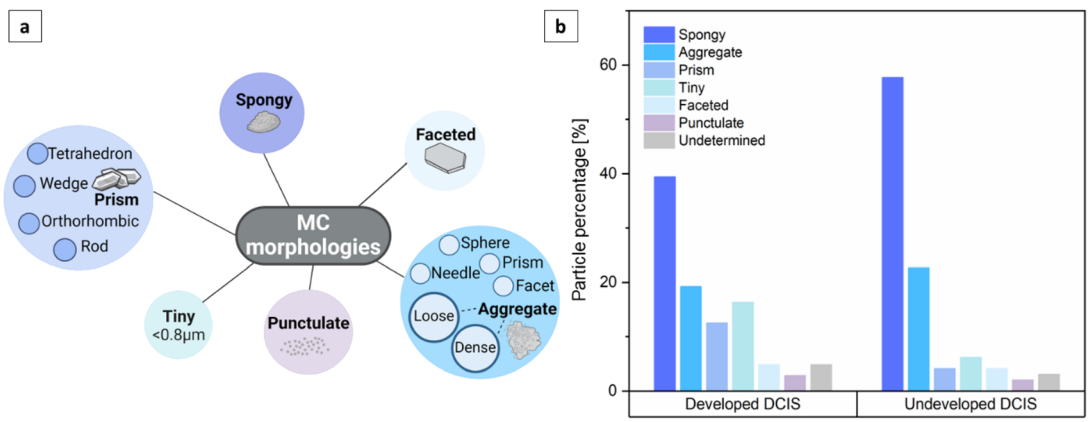

Fig. 3 (a) Classification of MC morphologies detected by SEM imaging. (b) Distribution of MCs based on their morphology, as detected by SEM imaging.

An examination of the distribution of MCs into the different categories (Fig. 3b) revealed that the majority of MCs were spongy particles, constituting 39.4% of the MCs in developed DCIS tissues and 57.7%, in undeveloped DCIS tissues. Aggregates were the second most numerous particles, comprising 19.2% and 22.7% of the MCs in developed and undeveloped DCIS tissues, respectively. MCs with prismatic morphologies and tiny particles were more common in developed DCIS cases (12.5% and 16.3%, respectively) than in undeveloped cases (4.1% and 6.2%, respectively). MCs with faceted and punctulate morphologies appeared in the tissues with a low incidence, with no particular relationship to DCIS progression. Punctulate particles were observed exclusively when the EDS analysis indicated the presence of phosphorus within the microstructure. Particles with undetermined morphologies correspond to MCs that were either damaged during imaging or concealed within tissue folds or in the matrix, rendering it challenging to precisely locate their surfaces. No clear correlation between breast MC morphology and DCIS progression could be concluded from these distributions.

3.2 MC elemental composition

After mineral particles in the tissues had been identified by backscattered electron detection, the elemental composition of the MCs was characterized through EDS measurements, with particular emphasis on the presence of calcium, phosphorus, and magnesium, since these three elements provide insights into the types of MC present in the different tissues. We regarded a chemical element as present in an MC when its detected value exceeded 0.7 wt%. The EDS analysis demonstrated two distinct compositions of MCs: those containing calcium and phosphorus (CaP MCs) and those containing calcium but no phosphorus (non-CaP MCs; Fig. S1†). Of the representative MCs shown in Fig. 2, almost half of the non-CaP MCs contained Mg, and notably, only one contained CaP (Table 2).

Table 2 Elemental composition of the MCs featured in Fig. 2 as determined by EDS analysis, expressed in molar percentages

Reference to Fig. 2	Calcium (%)	Magnesium (%)	Phosphorus (%)
a	96.8	0	0
b1	94.3	0	0
b2	37.9	30.3	0
b3	46.3	40.4	0
c	90.9	0	0
d	48.0	20.0	0
e	48.8	0	25.6
f	94.5	0	0

Overall, most of the MCs identified through SEM-EDS analysis were non-CaP, appearing in 88.1% of cases (177/201 MCs), while CaP MCs appeared only in 11.9% of cases (Table 3). Putative CaP crystals exhibiting a Ca : P molar ratio of 1.3–1.9 were observed only in 3.0% of the cases (6/201 MCs). The presence of phosphorus in MCs was infrequent, in contrast to previous studies that primarily identified CaP crystals in breast tissues. It was this finding that motivated us to focus on the crystal properties of non-CaP MCs.

Magnesium-containing MCs were identified in 28.2% (50/177) of all non-CaP MCs analyzed by EDS. These MCs appeared in both tumorous and normal tissues and for both developed and undeveloped DCIS, although less frequently in undeveloped DCIS patient tissues (Table 3). Of the total non-CaP MCs, 13% (23/177) had a Ca : Mg molar ratio of 1 ± 0.1, indicating that they are composed of dolomite. Most of these MCs appeared as spongy, prismatic, or tiny particles (Fig. 4), although some exhibited a faceted octahedral morphology resembling that of geological dolomite minerals (Fig. 4b, and S2†). The remainder of the Mg-containing non-CaP MCs had significantly lower Mg fractions, giving higher Ca : Mg molar ratios ranging from 5.3 to 32. These minerals were probably Mg-rich calcium carbonate or calcium oxalate crystals. Finally, 3.5% (7/201) of the total MCs analyzed with EDS were CaP minerals that also contained Mg, in percentages ranging between 2.6 and 19.3 wt%.

3.3 Crystal phase characterization of non-CaP MCs by Raman spectroscopy

Since Raman spectroscopy may be applied to distinguish between different types of mineral, it was particularly valuable for distinguishing between calcium carbonate, calcium oxalate and apatitic mineral phases, which cannot be differentiated through SEM and histology alone. Unlike most other studies in the field,[14,16,17,29,30] the sections used for Raman characterization in this study were not exposed to solvents, since they had not undergone paraffin embedding or ethanol dehydration/rehydration cycles, and the MCs were therefore less affected by the tissue preparation procedure. The Raman microscope used here allowed us to acquire measurements at a spatial resolution of approximately 0.4–0.7 μm according to the Rayleigh criterion. A cross-polarized system was used for the white light in the Raman microscope to locate MCs embedded within the tissue samples (Fig. 5a). These crystals typically appeared as

Table 3 Elemental composition distribution of DCIS MCs based on EDS analysis

Frequency of MC appearance, according to MC type	%
Non-CaP MCs out of total MCs	88.1
MCs containing Mg out of non-CaP MCs	28.2
MCs with Ca : Mg molar ratio of 1 (±0.1) out of non-CaP MCs	13.0
MCs containing Mg out of non-CaP MCs in developed DCIS cases	41.6
MCs containing Mg out of non-CaP MCs in undeveloped DCIS cases	17.2

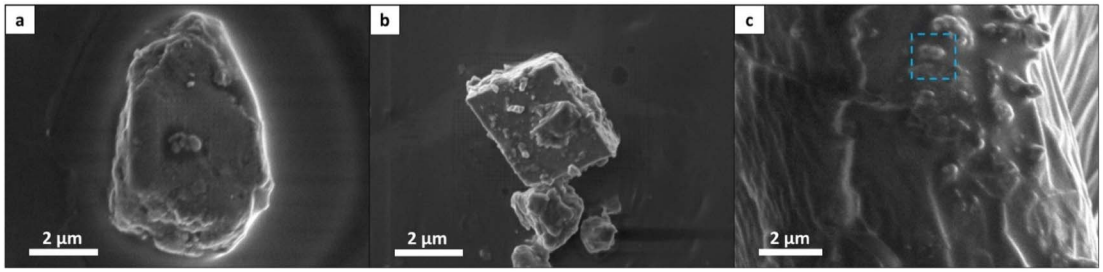

Fig. 4 Morphology of Mg-containing non-CaP MCs with Ca : Mg molar ratios of 1 ± 0.1. (a) Spongy morphology with a Ca : Mg molar ratio of 0.98, (b) prismatic morphology with a Ca : Mg molar ratio of 1.03. (c) Tiny MC with a Ca : Mg molar ratio of 1.1.

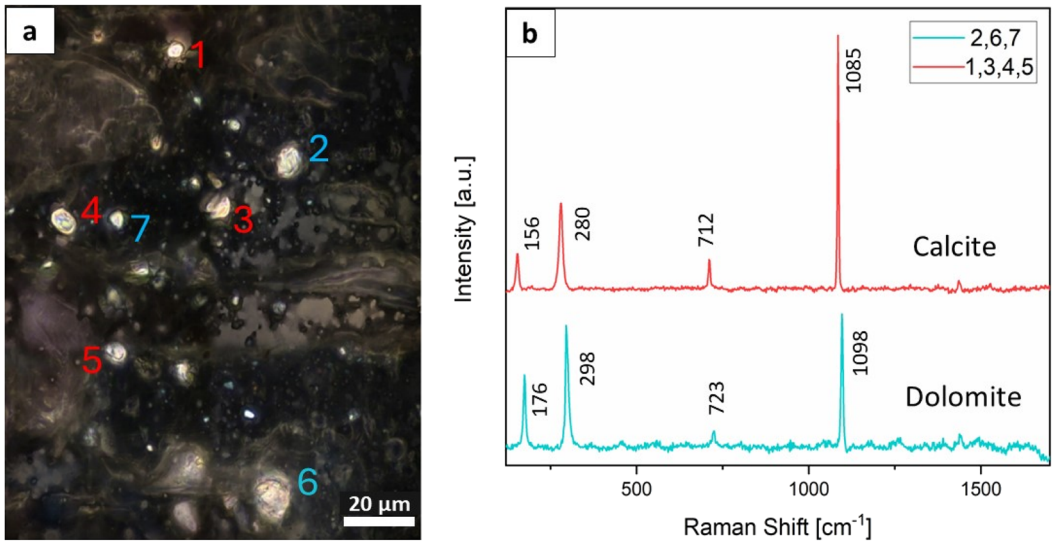

Fig. 5 Raman microscopy characterization of a normal tissue from a patient with developed DCIS. (a) White light image of the tissue. The numbers indicate the regions from which Raman spectra were obtained. (b) Representative spectra of calcite and dolomite detected in the regions numbered in (a).

birefringent particles. The employed resolution proved effective in detecting small MCs within the tissues. Raman spectroscopy confirmed that these small MCs, typically one to a few micrometers in size, were distributed in both normal and tumorous breast tissue. Since mammography has a less sensitive spatial resolution of 50 μm,[31] SEM imaging and Raman mapping may be used as complementary methods for identifying microscopic calcifications that may not be detected using mammography. Most MCs, as detected through both SEM imaging and Raman microscopy, were smaller than 5 μm, with well-defined boundaries and surfaces. Importantly, the MCs were observed embedded within the tissue in their original spatial context at microscopic scales; this finding indicates that they were not residual microscopic fragments resulting from the fracture of larger calcifications, but rather distinct individual MCs, exhibiting diverse morphologies. After imaging and size determination, Raman spectroscopy was performed to determine the composition and crystal phase of the MCs (Fig. 5b).

For the 197 MCs analyzed by Raman spectroscopy, only non-CaP MCs, specifically calcium carbonate crystals, were identified within the tissues (Table 4). These calcium carbonate MCs were distributed over tens of micrometers within the tissues, while no CaP or calcium oxalate MCs were detected. In some cases, mostly for small MCs, the spectra exhibited additional peaks corresponding to organic materials, including carotene and lipids. These molecules were probably incorporated inside the MCs or were located in the crystal microenvironment (Fig. S3†).

Our efforts with both cross-polarized and non-polarized light to locate CaP MCs led consistently to the discovery of calcium carbonate minerals exclusively. These crystals were found in

Table 4 Crystal phase distribution of DCIS MCs based on Raman spectroscopy

Frequency of MC appearance, according to MC type	%
Non-CaP MCs out of total MCs	100.0
Dolomite MCs out of total MCs	16.8
Calcite MCs out of total MCs	83.2
Dolomite MCs in developed DCIS cases	19.1
Dolomite MCs in undeveloped DCIS cases	14.6

normal and tumorous tissues in both developed and undeveloped DCIS cases. An unexpected finding was that the MCs consisted entirely of calcite ($CaCO_3$) and dolomite ($CaMg(CO_3)_2$). Raman spectra showed the characteristic peaks for calcite and dolomite: namely, for calcite, the ν_4 peak for symmetric CO_3^{2-} deformation at 712 cm^{-1}, the ν_1 peak for symmetric CO_3^{2-} stretching at 1085 cm^{-1}, and the translational lattice modes of calcium and carbonate ions at 156 and 280 cm^{-1} (Fig. 5b); and for dolomite, the ν_1 peak for symmetric CO_3^{2-} stretching at 1098 cm^{-1}, the ν_2 peak for CO_3^{2-} bending at 723 cm^{-1}, and the translational lattice modes of calcium and carbonate ions at 176 and 298 cm^{-1}.[32,33]

According to the Raman spectroscopy, calcite MCs in the tissues were more prevalent than dolomite MCs, with dolomite being detected in 16.8% of the measured MCs (Table 4). Among tissues obtained from patients with DCIS that developed into invasive cancer, dolomite accounted for 19.1% of the detected MCs, while calcite comprised 80.9%. Conversely, tissues from patients with DCIS that did not progress into invasive cancer showed a prevalence of 14.6% dolomite and 85.4% calcite. The dolomite : calcite ratio was higher (0.24) for developed DCIS cases and lower (0.17) for undeveloped cases. However, the statistical significance of these trends could not be analyzed due to the limited number of patients involved in this study, as described above. Nevertheless, these findings suggest that the presence and prevalence of dolomite, together with calcite, could potentially reveal pathologically relevant tissue changes and that the dolomite : calcite ratio could serve as an indicator of the DCIS progression potential.

To verify the presence of dolomite and to ensure that the material detected was not magnesium-rich calcite, we performed Raman spectroscopy on lab-synthesized Mg-calcite, biogenic Mg-calcite obtained from sea urchin tests, and dolomite powder extracted from mineral ore (Fig. 6). We then compared these spectra with the spectra obtained from the breast MCs. Our analysis demonstrated that the spectra of the synthetic and biogenic Mg-calcites differed from the spectrum of the dolomite MCs, while the geological dolomite spectrum was similar to the latter spectrum—findings also supported by the corresponding peak locations (Table S2†). In addition, an examination of the Raman peaks revealed comparable peak locations for the MC calcite and commercial calcite (Table S2†). These findings demonstrate the consistent presence of dolomite and calcite MCs in DCIS breast tissues and show for the first time, to the best of our knowledge, the presence of dolomite deposits in human breast DCIS tissue.

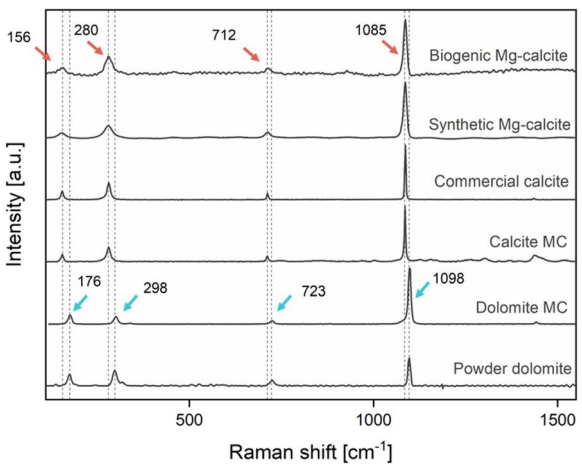

Fig. 6 Raman spectroscopy of dolomite and calcite MCs compared to powdered dolomite extracted from mineral ore, commercial calcite, biogenic magnesium-rich calcite obtained from sea urchin tests, and lab-synthesized Mg-calcite with a 6.5 wt% of magnesium verified by EDS analysis.

4. Discussion

The complexity and broad biochemical features of breast cancer and the diverse clinical outcomes of DCIS make it challenging to predict DCIS prognosis. Breast MCs potentially possess valuable information regarding the nature of DCIS, and much attention has been directed toward understanding the link between CaP MCs and malignancy in general. In this retrospective study, we utilized a combination of Raman spectroscopy and SEM-EDS to characterize breast MCs embedded within breast tissue sections obtained from DCIS patients. This approach enabled us to extend the information obtained from mammography and histopathology toward enriching our understanding of DCIS pathology. We established distinct biomineralogical fingerprints for 398 MCs from six patients. Using SEM imaging and EDS analysis, we localized 201 MCs within their original spatial context and classified their morphology, particle size, and elemental composition. Using Raman spectroscopy, we identified 197 MCs embedded within the DCIS tissue sections and obtained their size, composition, and crystal phases. Several Raman spectra of MCs revealed the presence of organic molecules, such as the pigment carotene and lipids. Most probably, some of these molecules were incorporated within the MCs, while others originated in their proximate surroundings. This finding aligns with prior studies in the field, which also detected organic materials, such as carotenes, lipids, and proteins, within and around MCs.[13,14,18]

The SEM examination of 201 MCs showed heterogeneity in morphology and particle size, as was to be expected given that these MCs are biominerals. Tissue constitutes a diverse and ever-changing biological environment, where crystal nucleation, growth, and aggregation processes are affected by physiological and chemical fluctuations.[34–37] Most MCs were smaller than 5 μm and exhibited spongy and aggregated morphologies, with the MCs found in developed *vs.* undeveloped DCIS tissue having a lower percentage of spongy particles.

Overall, 94% of the characterized MCs comprised non-CaP minerals, a finding contrasting with the typically high prevalence of CaP MCs previously reported in most breast tissue samples. Notably, in many studies on breast MCs, the tissue was subjected to fairly aggressive preparation protocols, including exposure to solvents, dehydration–rehydration processes, and elevated temperatures for paraffin or resin embedding.[14–17,19,20,29,30,38] However, minimally treated tissue, as was the case in this study, may be more suitable for

characterization and analysis.[39] Our finding of a low prevalence of CaP MCs can also be explained in terms of our use of DCIS tissue exclusively, whereas many studies examining the properties of breast MCs covered a broad range of malignancies, including invasive and metastatic cancers.[13–15,18,20,38]

We found no evidence for the presence of calcium oxalate minerals, possibly because calcium oxalate dihydrate MCs are typically not found in DCIS lesions, but are more commonly associated with benign breast conditions. Nonetheless, we cannot rule out the possibility that some of the calcite minerals observed using Raman spectroscopy originated from calcium oxalate minerals, which are known to undergo thermal decomposition to calcium carbonate.[40] Of the non-CaP MCs within DCIS breast tissue samples, we found only calcium carbonate minerals in the form of calcite and dolomite.

Calcite is a common component of the skeletons of many marine creatures and has been reported in pathological calcifications in human tissues.[41,42] While calcite has previously been identified in human tissue in the context of breast MCs (although this finding appeared to lack clinical significance[14,24,27]), dolomite has, to the best of our knowledge, not previously been detected in tumorous MCs; rather, it is primarily associated with geological sediments. Its presence in animals and humans has been documented only rarely, even though there are some reports suggesting dolomite formation in urinary stones.[43,44]

Dolomite is commonly found in cave and marble formations, coral reefs, and saline and hypersaline lakes. It typically forms through the alteration of calcium carbonate minerals in specific geological environments, with its formation being prolonged and complex and occurring under high pressure and temperatures, making it challenging to replicate in a laboratory setting.[45] Dolomite has a distinctive mineral structure, characterized by a well-ordered and specific organization within its Ca^{2+} and Mg^{2+} cation layers, which are separated into entirely distinct planes.[46] However, natural dolomite sometimes deviates from this stoichiometric composition, resulting in a lower-order arrangement known as protodolomite.[47] Even after decades of research, an ongoing debate persists regarding the exact mechanisms responsible for the development of sedimentary dolomite, both in its mineral and rock forms in the various environments in which it is found.[45] This ongoing debate, often dubbed "the dolomite problem" in geology and environmental science, arises from the incomplete understanding of how the dolomite's unique ordered structure forms under natural conditions.

Our finding of dolomite in a biological tissue indicates that ordered dolomite can nonetheless develop relatively quickly, even under physiological conditions. Although the synthesis of dolomite in a laboratory setting poses challenges, studies have indicated that dolomite minerals can precipitate at room temperature in the presence of microbes[48,49] or in the presence of catalysts, such as polysaccharides, ethanol, or exopolymeric substances produced by microorganisms like bacteria and algae.[50,51] In addition, microbial community activity has been found to encourage dolomite formation under ambient and low pH conditions within marine pore systems and living coralline algae.[52,53] Indeed, a recent study showed that pH fluctuations can induce cycles of dolomite undersaturation and supersaturation, potentially leading to dolomite formation under ambient conditions.[54] Similarly, solid tumors often display an acidic microenvironment and/or pH fluctuations as a consequence of the altered metabolism and the physiology of the cells within the tumor.[55] The above reports, together with our findings, suggest that a localized DCIS environment, possibly involving microorganism activity or pH fluctuations, could provide the conditions suitable for dolomite formation.

Both elemental composition and crystal phase analysis showed a higher prevalence of Mg-containing non-CaP MCs, specifically dolomite, in developed cases of DCIS compared to undeveloped cases (18.0% and 8.0% MCs with a Ca : Mg molar ratio of 1 ± 0.1 out of total non-CaP MCs in developed and undeveloped cases, respectively, analyzed *via* EDS). These findings offer valuable insights into the chemical characteristics of non-CaP breast MCs in DCIS and highlight the potential of Mg content, in particular, dolomite, as an indicator of DCIS progression.

We note that this study has a few limitations. First, it was conducted on a small number of samples, and therefore lacks statistical power. Second, there were some limitations regarding the source of tissue samples: despite the diverse origins of the patients examined and treated in various medical facilities, all the samples were collected in a single country. Additionally, due to the limited number of patients, the extensive clinical information collected for each patient could not be leveraged for statistical analysis, and therefore several clinical parameters were not taken into consideration when searching for correlations with the MC crystal properties (with the exception of their retrospective development status). Notably, the wide range of ages of the patients is a factor that may potentially influence the development or recurrence status of each individual patient.[56] In addition, all patients underwent treatment following the biopsy procedure and tissue collection. Therefore, one of the most influential factors in illness development, namely, treatment, was not taken into consideration in the analysis. Consequently, we can assert with confidence that cases where DCIS developed even with treatment would also be developed without the treatment, but we could not ascertain, with sufficient certainty, whether the absence of DCIS development was due to specific treatment procedures.

Through the integration of spectroscopic techniques and minimal tissue processing, this study offers new insights into the composition and morphology of MCs within DCIS tissue. Our analytical approach not only shows potential of utilizing non-CaP MCs for a deeper understanding of DCIS beyond screening applications but also establishes the groundwork for deeper insights into the biomineralization mechanisms responsible for the formation of dolomite minerals under physiological conditions.

5. Conclusions

In this retrospective study, MCs embedded within tissue sections obtained from DCIS patients were characterized using SEM-EDS and Raman spectroscopy. The patients had been diagnosed between the years 2014 and 2019, and their current health status, particularly whether DCIS developed into invasive

cancer over time, was included in our analysis. The morphology, particle size, elemental composition, and crystal phase were characterized for 398 MCs obtained from six patients. The tissue processing protocol did not involve exposure of the tissues to solvents or heating; instead, it included cryo-sectioning, air drying, and rinsing with water. Most of the MCs identified comprised non-CaP minerals, namely, calcite and dolomite, and exhibited heterogeneous morphologies.

For the first time, to the best of our knowledge, dolomite was identified within the tumorous tissue; it was probably formed in response to fluctuations in the chemical milieu of the tumor microenvironment. Due to the limited availability of DCIS samples, the study included only six patients, making statistical analysis unfeasible. Nonetheless, our findings indicate that both in patients where DCIS progressed into invasive cancer and in those where it did not, the majority of MCs analyzed consisted of calcite. Furthermore, the dolomite-to-calcite ratio was higher in cases where DCIS developed compared to those where it did not. This suggests that an increased prevalence of dolomite in DCIS tissues might correlate with poorer health outcomes. Future research involving a larger patient cohort should further explore the potential prognostic value of dolomite MCs.

Data availability statement

The data supporting this article have been included as part of the ESI.†

Conflicts of interest

There are no conflicts to declare.

Acknowledgements

This work was supported by the Israel Science Foundation [grant number 565/21]. The authors thank Prof. Shimon Reisner, Edna Sebag, and MIDGAM national tissue bank staff for providing the tissue samples, clinical data, and medical follow-ups. The authors also thank Roxana Golan for her help with SEM imaging, Prof. Lia Addadi for providing a reference sea urchin test, Dr Ishai Luz for his help with tissue sectioning, and Rebecca Willson for providing the dolomite sample. NV is the incumbent of the Joseph and May Winston Career Development Chair in Chemical Engineering. The illustrations were created with https://www.biorender.com/.

References

1 C. I. Li, D. J. Uribe and J. R. Daling, Clinical Characteristics of Different Histologic Types of Breast Cancer, *Br. J. Cancer*, 2005, **93**(9), 1046–1052, DOI: 10.1038/sj.bjc.6602787.

2 M. Akram, M. Iqbal, M. Daniyal and A. U. Khan, Awareness and Current Knowledge of Breast Cancer, *Biol. Res.*, 2017, **50**(1), 33, DOI: 10.1186/s40659-017-0140-9.

3 S. O'Grady and M. P. Morgan, Microcalcifications in Breast Cancer: From Pathophysiology to Diagnosis and Prognosis, *BBA, Biochim. Biophys. Acta, Rev. Cancer*, 2018, **1869**(2), 310–320, DOI: 10.1016/j.bbcan.2018.04.006.

4 S. Hofvind, B. Iversen, L. Eriksen, B. Styr, K. Kjellevold and K. Kurz, Mammographic Morphology and Distribution of Calcifications in Ductal Carcinoma *in Situ* Diagnosed in Organized Screening, *Acta Radiol.*, 2011, **52**(5), 481–487, DOI: 10.1258/ar.2011.100357.

5 E. J. Groen, J. Hudecek, L. Mulder, M. Van Seijen, M. M. Almekinders, S. Alexov, A. Kovács, A. Ryska, Z. Varga, F.-J. Andreu Navarro, S. Bianchi, W. Vreuls, E. Balslev, M. V. Boot, J. Kulka, E. Chmielik, E. Barbé, M. J. De Rooij, W. Vos, A. Farkas, N. E. Leeuwis-Fedorovich, P. Regitnig, P. J. Westenend, L. F. S. Kooreman, C. Quinn, G. Floris, G. Cserni, P. J. Van Diest, E. H. Lips, M. Schaapveld and J. Wesseling, Prognostic Value of Histopathological DCIS Features in a Large-Scale International Interrater Reliability Study, *Breast Cancer Res. Treat.*, 2020, **183**(3), 759–770, DOI: 10.1007/s10549-020-05816-x.

6 L. L. Visser, E. J. Groen, F. E. Van Leeuwen, E. H. Lips, M. K. Schmidt and J. Wesseling, Predictors of an Invasive Breast Cancer Recurrence after DCIS: A Systematic Review and Meta-Analyses, *Cancer Epidemiol., Biomarkers Prev.*, 2019, **28**(5), 835–845, DOI: 10.1158/1055-9965.EPI-18-0976.

7 M.-F. Yen, L. Tabár, B. Vitak, R. A. Smith, H.-H. Chen and S. W. Duffy, Quantifying the Potential Problem of Overdiagnosis of Ductal Carcinoma *in Situ* in Breast Cancer Screening, *Eur. J. Cancer*, 2003, **39**(12), 1746–1754, DOI: 10.1016/S0959-8049(03)00260-0.

8 B. Erbas, E. Provenzano, J. Armes and D. Gertig, The Natural History of Ductal Carcinoma *in Situ* of the Breast: A Review, *Breast Cancer Res. Treat.*, 2006, **97**(2), 135–144, DOI: 10.1007/s10549-005-9101-z.

9 S. E. Pinder, A. M. Thompson and J. Wesserling, Low-Risk DCIS. What Is It? Observe or Excise?, *Virchows Arch.*, 2022, **480**(1), 21–32, DOI: 10.1007/s00428-021-03173-8.

10 M. Morrow, E. A. Strom, L. W. Bassett, D. D. Dershaw, B. Fowble, J. R. Harris, F. O'Malley, S. J. Schnitt, S. E. Singletary and D. P. Winchester, Standard for the Management of Ductal Carcinoma *In Situ* of the Breast (DCIS), *Ca-Cancer J. Clin.*, 2002, **52**(5), 256–276, DOI: 10.3322/canjclin.52.5.256.

11 E. J. Groen, L. E. Elshof, L. L. Visser, E. J. Th. Rutgers, H. A. O. Winter-Warnars, E. H. Lips and J. Wesseling, Finding the Balance between Over- and under-Treatment of Ductal Carcinoma *in Situ* (DCIS), *Breast*, 2017, **31**, 274–283, DOI: 10.1016/j.breast.2016.09.001.

12 S. Gosling, D. Calabrese, J. Nallala, C. Greenwood, S. Pinder, L. King, J. Marks, D. Pinto, T. Lynch, I. D. Lyburn, E. S. Hwang, K. Rogers and N. Stone, A Multi-Modal Exploration of Heterogeneous Physico–Chemical Properties of DCIS Breast Microcalcifications, *Analyst*, 2022, **147**, 1641–1654, DOI: 10.1039/D1AN01548F.

13 J. A. M. R. Kunitake, S. Choi, K. X. Nguyen, M. M. Lee, F. He, D. Sudilovsky, P. G. Morris, M. S. Jochelson, C. A. Hudis, D. A. Muller, P. Fratzl, C. Fischbach, A. Masic and L. A. Estroff, Correlative Imaging Reveals Physiochemical

Heterogeneity of Microcalcifications in Human Breast Carcinomas, *J. Struct. Biol.*, 2018, **202**(1), 25–34, DOI: 10.1016/j.jsb.2017.12.002.

14 R. Vanna, C. Morasso, B. Marcinnò, F. Piccotti, E. Torti, D. Altamura, S. Albasini, M. Agozzino, L. Villani, L. Sorrentino, O. Bunk, F. Leporati, C. Giannini and F. Corsi, Raman Spectroscopy Reveals That Biochemical Composition of Breast Microcalcifications Correlates with Histopathologic Features, *Cancer Res.*, 2020, **80**(8), 1762–1772, DOI: 10.1158/0008-5472.CAN-19-3204.

15 R. Scott, C. Kendall, N. Stone and K. Rogers, Elemental *vs.* Phase Composition of Breast Calcifications, *Sci. Rep.*, 2017, **7**(1), 136, DOI: 10.1038/s41598-017-00183-y.

16 A. Ben Lakhdar, M. Daudon, M.-C. Mathieu, A. Kellum, C. Balleyguier and D. Bazin, Underlining the Complexity of the Structural and Chemical Characteristics of Ectopic Calcifications in Breast Tissues through FE-SEM and μFTIR Spectroscopy, *C. R. Chim.*, 2016, **19**(11–12), 1610–1624, DOI: 10.1016/j.crci.2015.03.011.

17 A. S. Haka, K. E. Shafer-Peltier, M. Fitzmaurice, J. Crowe, R. R. Dasari and M. S. Feld, Identifying Microcalcifications in Benign and Malignant Breast Lesions by Probing Differences in Their Chemical Composition Using Raman Spectroscopy, *Cancer Res.*, 2002, **62**(18), 5375–5380.

18 J. A. M. R. Kunitake, D. Sudilovsky, L. M. Johnson, H.-C. Loh, S. Choi, P. G. Morris, M. S. Jochelson, N. M. Iyengar, M. Morrow, A. Masic, C. Fischbach and L. A. Estroff, Biomineralogical Signatures of Breast Microcalcifications, *Sci. Adv.*, 2023, **9**(8), eade3152, DOI: 10.1126/sciadv.ade3152.

19 S. B. Gosling, E. L. Arnold, S. K. Davies, H. Cross, I. Bouybayoune, D. Calabrese, J. Nallala, S. E. Pinder, L. Fu, E. H. Lips, L. King, J. Marks, A. Hall, L. J. Grimm, T. Lynch, D. Pinto, H. Stobart, E. S. Hwang, J. Wesseling, K. Geraki, N. Stone, I. D. Lyburn, C. Greenwood, K. D. Rogers, A. Thompson, S. Nik-Zainal, E. J. Sawyer, H. Davies, A. Futreal, N. Navin, J. Jonkers, J. van Rheenen, F. Behbod, M. Schmidt, L. F. A. Wessels, D. Rea, P. Bhattacharjee, D. Collyar, E. Verschuur and M. van Oirsouw, Microcalcification Crystallography as a Potential Marker of DCIS Recurrence, *Sci. Rep.*, 2023, **13**(1), 9331, DOI: 10.1038/s41598-023-33547-8.

20 R. Scott, N. Stone, C. Kendall, K. Geraki and K. Rogers, Relationships between Pathology and Crystal Structure in Breast Calcifications: An *in Situ* X-Ray Diffraction Study in Histological Sections, *npj Breast Cancer*, 2016, **2**(1), 16029, DOI: 10.1038/npjbcancer.2016.29.

21 R. Bonfiglio, M. Scimeca, N. Toschi, C. A. Pistolese, E. Giannini, C. Antonacci, S. Ciuffa, V. Tancredi, U. Tarantino, L. Albonici and E. R. Bonanno, Histological and Chemical Analysis of Breast Microcalcifications: Diagnostic Value and Biological Significance, *J. Mammary Gland Biol. Neoplasia*, 2018, **23**(1–2), 89–99, DOI: 10.1007/s10911-018-9396-0.

22 R. Baker, K. D. Rogers, N. Shepherd and N. Stone, New Relationships between Breast Microcalcifications and Cancer, *Br. J. Cancer*, 2010, **103**(7), 1034–1039, DOI: 10.1038/sj.bjc.6605873.

23 M. Scimeca, E. Giannini, C. Antonacci, C. A. Pistolese, L. G. Spagnoli and E. Bonanno, Microcalcifications in Breast Cancer: An Active Phenomenon Mediated by Epithelial Cells with Mesenchymal Characteristics, *BMC Cancer*, 2014, **14**(1), 286, DOI: 10.1186/1471-2407-14-286.

24 C. Morasso, R. Vanna, F. Piccotti, L. Frizzi, M. Truffi, S. Albasini, C. Borca, T. Huthwelker, L. Villani, O. Bunk, C. Giannini and F. Corsi, Whitlockite Has a Characteristic Distribution in Mammary Microcalcifications and It Is Not Associated with Breast Cancer, *Cancer Commun.*, 2023, **43**(10), 1169–1173, DOI: 10.1002/cac2.12481.

25 J. J. Going, T. T. Anderson, P. P. Crocker and D. D. Levison, Weddellite Calcification in the Breast: Eighteen Cases with Implications for Breast Cancer Screening, *Histopathology*, 2007, **16**(2), 119–124, DOI: 10.1111/j.1365-2559.1990.tb01079.x.

26 L. Frappart, M. Boudeulle, J. Boumendil, H. C. Lin, I. Martinon, C. Palayer, Y. Mallet-Guy, D. Raudrant, A. Bremond, Y. Rochet and J. Feroldi, Structure and Composition of Microcalcifications in Benign and Malignant Lesions of the Breast: Study by Light Microscopy, Transmission and Scanning Electron Microscopy, Microprobe Analysis, and X-Ray Diffraction, *Hum. Pathol.*, 1984, **15**(9), 880–889, DOI: 10.1016/S0046-8177(84)80150-1.

27 A. Fandos-Morera, M. Prats-Esteve, J. M. Tura-Soteras and A. Traveria-Cros, Breast Tumors: Composition of Microcalcifications, *Radiology*, 1988, **169**(2), 325–327, DOI: 10.1148/radiology.169.2.2845471.

28 R. Scott, I. Lyburn, E. Cornford, P. Bouzy, N. Stone, C. Greenwood, I. Bouybayoune, S. Pinder and K. Rogers, Breast Calcification Micromorphology Classification, *Br. J. Radiol.*, 2022, **95**(1139), 20220485, DOI: 10.1259/bjr.20220485.

29 A. S. Haka, K. E. Shafer-Peltier, M. Fitzmaurice, J. Crowe, R. R. Dasari and M. S. Feld, Diagnosing Breast Cancer by Using Raman Spectroscopy, *Proc. Natl. Acad. Sci. U.S.A.*, 2005, **102**(35), 12371–12376, DOI: 10.1073/pnas.0501390102.

30 Y. Zhang, C. Wang, Y. Li, A. Lu, F. Meng, H. Ding, F. Mei, J. Liu, K. Li, C. Yang, J. Du and Y. Li, Carbonate and Cation Substitutions in Hydroxylapatite in Breast Cancer Micro-Calcifications, *Min. Mag.*, 2021, **85**(3), 321–331, DOI: 10.1180/mgm.2021.23.

31 R. M. Rangayyan, T. M. Nguyen, F. J. Ayres and A. K. Nandi, Effect of Pixel Resolution on Texture Features of Breast Masses in Mammograms, *J. Digit. Imag.*, 2010, **23**(5), 547–553, DOI: 10.1007/s10278-009-9238-0.

32 S. Gunasekaran, G. Anbalagan and S. Pandi, Raman and Infrared Spectra of Carbonates of Calcite Structure, *J. Raman Spectrosc.*, 2006, **37**(9), 892–899, DOI: 10.1002/jrs.1518.

33 A. E. Murphy, R. S. Jakubek, A. Steele, M. D. Fries and M. Glamoclija, Raman Spectroscopy Provides Insight into Carbonate Rock Fabric Based on Calcite and Dolomite Crystal Orientation, *J. Raman Spectrosc.*, 2021, **52**(6), 1155–1166, DOI: 10.1002/jrs.6097.

34 N. Vidavsky, J. A. M. R. Kunitake and L. A. Estroff, Multiple Pathways for Pathological Calcification in the Human Body, *Adv. Healthcare Mater.*, 2021, **10**(4), 2001271, DOI: 10.1002/adhm.202001271.

35 S. Weiner and L. Addadi, Crystallization Pathways in Biomineralization, *Annu. Rev. Mater. Res.*, 2011, **41**(1), 21–40, DOI: 10.1146/annurev-matsci-062910-095803.

36 R. Gelli, V. Pucci, F. Ridi and P. Baglioni, A Study on Biorelevant Calciprotein Particles: Effect of Stabilizing Agents on the Formation and Crystallization Mechanisms, *J. Colloid Interface Sci.*, 2022, **620**, 431–441, DOI: 10.1016/j.jcis.2022.04.025.

37 L. N. Poloni and M. D. Ward, The Materials Science of Pathological Crystals, *Chem. Mater.*, 2014, **26**(1), 477–495, DOI: 10.1021/cm402552v.

38 S. Gosling, R. Scott, C. Greenwood, P. Bouzy, J. Nallala, I. D. Lyburn, N. Stone and K. Rogers, Calcification Microstructure Reflects Breast Tissue Microenvironment, *J. Mammary Gland Biol. Neoplasia*, 2019, **24**(4), 333–342, DOI: 10.1007/s10911-019-09441-3.

39 C. Gassner, J. A. Adegoke, S. K. Patel, V. J. Sharma, K. Kochan, L. M. Burrell, J. Raman and B. R. Wood, Improved Tissue Preparation for Multimodal Vibrational Imaging of Biological Tissues, *Clin. Spectrosc.*, 2022, **4**, 100021, DOI: 10.1016/j.clispe.2022.100021.

40 D. Hourlier, Thermal Decomposition of Calcium Oxalate: Beyond Appearances, *J. Therm. Anal. Calorim.*, 2019, **136**(6), 2221–2229, DOI: 10.1007/s10973-018-7888-1.

41 H. Colboc, P. Moguelet, D. Bazin, C. Bachmeyer, V. Frochot, R. Weil, E. Letavernier, C. Jouanneau, M. Daudon and J. F. Bernaudin, Physicochemical Characterization of Inorganic Deposits Associated with Granulomas in Cutaneous Sarcoidosis, *J. Eur. Acad. Dermatol. Venereol.*, 2019, **33**(1), 198–203, DOI: 10.1111/jdv.15167.

42 V. Frochot, V. Castiglione, I. T. Lucas, J.-P. Haymann, E. Letavernier, D. Bazin, G. B. Fogazzi and M. Daudon, Advances in the Identification of Calcium Carbonate Urinary Crystals, *Clin. Chim. Acta*, 2021, **515**, 1–4, DOI: 10.1016/j.cca.2020.12.024.

43 C. F. Mansfield, A Urolith of Biogenic Dolomite-Another Clue in the Dolomite Mystery, *Geochim. Cosmochim. Acta*, 1980, **44**(6), 829–839, DOI: 10.1016/0016-7037(80)90264-1.

44 M. H. Gault, L. Chafe, L. Longerich and R. A. Mason, Calcium and Calcium Magnesium Carbonate Specimens Submitted as Urinary Tract Stones, *J. Urol.*, 1993, **149**(2), 244–249, DOI: 10.1016/S0022-5347(17)36047-0.

45 J. M. Gregg, D. L. Bish, S. E. Kaczmarek and H. G. M. Machel, Nucleation and Growth of Dolomite in the Laboratory and Sedimentary Environment: A Review, *Sedimentology*, 2015, **62**(6), 1749–1769, DOI: 10.1111/sed.12202.

46 J. Sun, Z. Wu, H. Cheng, Z. Zhang and R. L. Frost, A Raman Spectroscopic Comparison of Calcite and Dolomite, *Spectrochim. Acta, Part A*, 2014, **117**, 158–162, DOI: 10.1016/j.saa.2013.08.014.

47 J. D. Rodriguez-Blanco, S. Shaw and L. G. Benning, A Route for the Direct Crystallization of Dolomite, *Am. Mineral.*, 2015, **100**(5–6), 1172–1181, DOI: 10.2138/am-2015-4963.

48 C. Vasconcelos, J. McKenzie, S. Bernasconi, D. Grujic and A. J. Tiens, Microbial Mediation as a Possible Mechanism for Natural Dolomite Formation at Low Temperatures, *Nature*, 1995, **377**, 220–222, DOI: 10.1038/377220a0.

49 M. Sánchez-Román, C. S. Romanek, D. C. Fernández-Remolar, A. Sánchez-Navas, J. A. McKenzie, R. A. Pibernat and C. Vasconcelos, Aerobic Biomineralization of Mg-Rich Carbonates: Implications for Natural Environments, *Chem. Geol.*, 2011, **281**(3–4), 143–150, DOI: 10.1016/j.chemgeo.2010.11.020.

50 P. Del Buey and M. E. Sanz-Montero, Biomineralization of Ordered Dolomite and Magnesian Calcite by the Green Alga *Spirogyra*, *Sedimentology*, 2023, **70**(3), 685–704, DOI: 10.1111/sed.13046.

51 C. Zhou, S. Jin, Z. Sun, A. Homkrajae, E. Myagkaya, N. Nilpetploy and K. Lawanwong, Disordered Dolomite as an Unusual Biomineralization Product Found in the Center of a Natural Cassis Pearl, *PLoS One*, 2023, **18**(4), e0284295, DOI: 10.1371/journal.pone.0284295.

52 J. M. Rivers, Warm Acidified Seawater: A Dolomite Solution, *J. Sediment. Res.*, 2023, **93**(3), 187–201, DOI: 10.2110/jsr.2022.087.

53 G. Diaz-Pulido, M. C. Nash, K. R. N. Anthony, D. Bender, B. N. Opdyke, C. Reyes-Nivia and U. Troitzsch, Greenhouse Conditions Induce Mineralogical Changes and Dolomite Accumulation in Coralline Algae on Tropical Reefs, *Nat. Commun.*, 2014, **5**(1), 3310, DOI: 10.1038/ncomms4310.

54 J. Kim, Y. Kimura, B. Puchala, T. Yamazaki, U. Becker and W. Sun, Dissolution Enables Dolomite Crystal Growth near Ambient Conditions, *Science*, 2023, **382**(6673), 915–920, DOI: 10.1126/science.adi3690.

55 E. Boedtkjer and S. F. Pedersen, The Acidic Tumor Microenvironment as a Driver of Cancer, *Annu. Rev. Physiol.*, 2020, **82**(1), 103–126, DOI: 10.1146/annurev-physiol-021119-034627.

56 P. A. Cronin, C. Olcese, S. Patil, M. Morrow and K. J. Van Zee, Impact of Age on Risk of Recurrence of Ductal Carcinoma *In Situ*: Outcomes of 2996 Women Treated with Breast-Conserving Surgery Over 30 Years, *Ann. Surg Oncol.*, 2016, **23**(9), 2816–2824, DOI: 10.1245/s10434-016-5249-5.